Soft Matter

Cite this: *Soft Matter*, 2012, **8**, 6128

www.rsc.org/softmatter

PAPER

Mapping fluctuations in biomembranes adhered to micropatterns†

Cornelia Monzel,*[ab] Susanne F. Fenz,‡[a] Margret Giesen,[a] Rudolf Merkel[a] and Kheya Sengupta*[b]

Received 23rd December 2011, Accepted 2nd April 2012
DOI: 10.1039/c2sm07458c

We studied biomembrane fluctuations by calculating the instantaneous shape of model membranes adhered to micro-patterned substrates, using micro-interferometry. The model consisted of partially adherent giant unilamellar vesicles (GUVs) which were osmotically deflated. Adhesion was effected *via* the specific ligand–receptor interaction of biotin–neutravidin. Special micro-structured adhesive substrates were developed where the receptors were distributed in the form of grids or lines. Dual-wavelength reflection interference contrast microscopy (DW-RICM) measurements revealed that on the structured adhesive substrates GUVs exhibit regions of bound and fluctuating membrane, in accordance with the underlying pattern. In the fluctuating zone, the membrane presented itself as a flat-topped hill for an initial osmotic difference of 70 mOsm l^{-1}. The membrane–substrate distance saturated at a plateau of 79 ± 9 nm. In this plateau, the fluctuation amplitude was found to be 10 ± 3 nm. Variation of the shape (grid *versus* lines) or size (grids of 3.5 or 7 μm lattice constant) influenced neither the height nor the fluctuation amplitude in the plateau. Fourier analysis revealed that the mode corresponding to a wavelength of twice the pattern size always contributed, and, depending on the substrate, additional modes were sometimes present. The plateau height could be tuned from 0 to 538 nm by changing the initial osmotic gradient between the inside and outside of the GUV, which effectively tuned the membrane tension. The corresponding fluctuation amplitude ranged from non-detectable to a maximum of 17 nm. Our results can be interpreted in the light of a tension dependent effective interaction potential.

1 Introduction

Biological membranes are a classic example of soft fluctuating interfaces. In a living animal cell, the plasma membrane is in constant random motion—part of this arises from active processes in the cell but part of it is purely thermal. Early studies of such fluctuations in erythrocytes, which lack a nucleus and have only a rudimentary cytoskeleton proved to be puzzling to biologists who believed that all motion in biology is active.[1,2] Pioneering work from Brochard-Wyart and Lennon,[3] however, proved unambiguously that these fluctuations are mostly thermally driven. Recent results suggest an additional contribution from active processes under certain circumstances.[4] From the point of view of membrane physics, these thermal fluctuations are very important since they give rise to the so called Helfrich repulsion between soft uncharged membranes purely due to entropic reasons.[5] While the theory of membrane fluctuations is believed to be well understood[6,7] and membrane shapes on different surface patterns have been modeled,[8] experiments have largely lagged behind. This is because there are very few convenient tools for measuring membrane fluctuations,[9] and fewer still offer the possibility of making a 2D map of the fluctuations across the entire membrane.[10]

Reflection interference contrast microscopy (RICM)[11,12] and fluorescence interference contrast microscopy (FLIC)[13] are two optical tools which are capable of mapping membrane fluctuations. RICM was used by Rädler and Sackmann[11] in early studies with GUVs where membrane fluctuations were measured quantitatively and compared with the theory in the limit of weakly adhering vesicles. As expected, a shallow minimum of the membrane to substrate interaction potential was detected. In an in-depth study on the Helfrich repulsion in two component systems, it was established that a dynamic phase separation of the components is coupled to the fluctuations.[14] More recent data on fluctuations of membranes, either decorated with polymers or close to a polymer coated surface, confirmed the notion of a metastable minimum in the potential. This was detected a few hundred nanometres above the substrate and an energy barrier was found that has to be crossed in order to access the stable minimum corresponding to true adhesion.[15,16] Fluctuations therefore play a crucial role in the nucleation of an adhesion

[a]*Institute of Complex Systems 7 (ICS-7), Forschungszentrum Jülich, Jülich, Germany. E-mail: c.monzel@fz-juelich.de*
[b]*CNRS UPR 3118 (Centre Interdisciplinaire de Nanosciences de Marseille - CINaM), Aix-Marseille Université, Marseille Cedex 9, France. E-mail: sengupta@cinam.univ-mrs.fr*

† Electronic Supplementary Information (ESI) available: micrographs of vesicle inflation experiments triggered by osmotic shock. See DOI: 10.1039/c2sm07458c

‡ Present address: Leiden Institute of Physics, Leiden University, 2333 CA Leiden, The Netherlands.

patch.[16] Groves and co-workers used FLIC to map the entire surface of a fluctuating membrane from a ruptured GUV.[17] They could elucidate hydrodynamic damping and predicted two types of membrane binding. These data are also consistent with the presence of a secondary minimum.

In addition, dynamic RICM spatial maps have been used in the semi-quantitative analysis of membrane fluctuations in cells[18,19] and vesicles,[20] as well as for diagnosing adhesion *via* dilute bond arrays not detectable otherwise.[21,22] In spite of all this progress, there has not been a systematic study of the influence of membrane parameters like tension or membrane confinement geometries on membrane fluctuations.

Here we have used dual-wavelength reflection interference contrast microscopy (DW-RICM) to monitor the membrane of a GUV in the vicinity of a substrate. The GUV adhered specifically to a well defined pattern and exhibited regions of bound and fluctuating membrane (see Fig. 1). Micro-contact printing enabled high control over the adhesive pattern and confined the membrane within specifically bound regions. While micro-contact printing is now almost routinely used for cell investigations,[23,24] its use in vesicle studies has so far been restricted. This is because, in the case of vesicles, unspecific attraction in the repulsive zones is difficult to screen.[25] Such partial adhesion of the membrane was a key factor here in enabling a quantitative comparison with theoretical expectations.

This also permitted us to study the effect of an osmotic imbalance in a systematic manner. Osmotic pressure differences are important for many biological functions. A striking example comes from the nephron in the urinary system, where the proximal convoluted tubule epithelium withstands pressure differences of up to 1 Osm l^{-1}, or the oesophagus epithelium, which constantly transports large amounts of fluid and electrolytes.[26–28] However, due to the lack of available experimental techniques, there is little understanding of the mechanisms brought into play during osmotic changes. Our experiments provide the first systematic view of the osmotic equilibration of adhered membranes and may shed light on the working of such tissues.

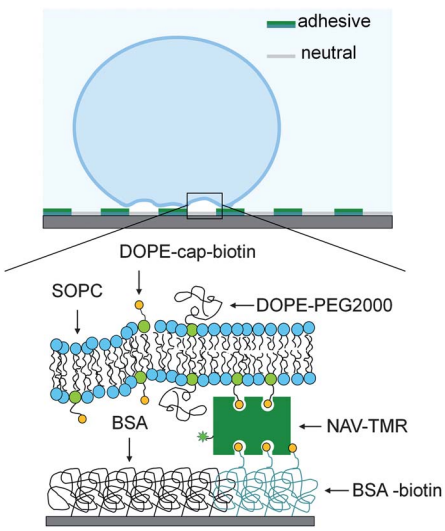

Fig. 1 A sketch illustrating the model system consisting of an osmotically deflated giant unilamellar vesicle (GUV) adhered to a patterned substrate. The vesicle membrane is made of a passive matrix lipid (SOPC and is doped with a headgroup modified lipid (DOPE), carrying PEG-polymers to prevent unspecific adhesion, and biotin linkers to mediate adhesion *via* NAV. The NAV protein with a fluorescent marker TMR is specifically bound to the substrate *via* BSA–biotin, which is micro-contact printed. The non-printed area is passivated with BSA. See text for preparation details and abbreviations of molecules.

2 Experimental

Materials

Lipids SOPC (1-stearoyl-2-oleoyl-sn-glycero-3-phosphocholine), DOPE–PEG 2000 (1,2-dioleoyl-sn-glycero-3-phosphoethanolamine-*N*-(methoxy(polyethyleneglycol)-2000)) and DOPE–cap-biotin (1,2-dioleoyl-sn-glycero-3-phosphoethanolamine-*N*-(cap biotinyl)) were purchased from Avanti Polar Lipids (Alabaster, AL, USA) and used without further purification. Neutravidin covalently linked to the fluorescent label tetramethylrhodamine, henceforth called NAV–TMR, (Invitrogen, Eugene, OR, USA) was reconstituted in PBS (phosphate buffered saline) buffer (140 mM NaCl, 3 mM KCl, 10 mM Na_2HPO_4, 2 mM KH_2PO_4, pH 7.2) and ultracentrifugated at 137 000 g and 4 °C for 2 h to eliminate protein aggregates. Bovine serum albumin (BSA) and its covalently linked biotin conjugate (both: Sigma, Saint Louis, MO, USA) were dissolved in ultrapure water to a final concentration of 0.1 mg mL^{-1} and mixed in a 1 : 1 w/w ratio (BSA–biotin mix). Ultrapure water was provided using a water purification system (Milli-Q Gradient A10, Millipore, San Francisco, CA, USA).

Thickness corrected glass coverslips (d = 170 ± 10 μm, Assistent, Karl Hecht KG, Sondheim, Germany), were cleaned by the following detergent treatment: ultrasonication in 2% Hellmanex solution (Hellma, Müllheim, Germany) for 10 min, flushing thoroughly with ultrapure water and again ultrasonication (2 × 15 min) in ultrapure water followed by repeated flushing with the same.

For the preparation of microstamps, pieces of polyolefin plastomer (POP, thickness 0.5 mm, 1 cm^2 size) were cleaned as above. Cross-linked polydimethylsiloxane (Sylgard 184, Dow Corning, USA), destined to form an inking pad, was prepared by mixing a base and curing agent in a ratio of 10 : 1 by weight (Young's modulus of ~3 MPa). Microstructured Si/SiO_2 wafers were prepared using UV lithography and reactive ion etching as described in detail by Cesa *et al.*[29] Three different structures of 1 cm^2 overall size were employed: (1) a large grid structure exhibiting a square lattice of 7 μm lattice constant and square shaped stubs of 4 μm width and 0.5 μm height, (2) a small grid with a square lattice of half the size (3.5 μm lattice constant, square shaped stubs of 2 μm width and 0.5 μm height) and (3) a line structure of 6 μm lattice constant, with 3.5 μm wide indentations and 2.5 μm wide elevations.

Sample preparation

Substrates with patterned receptor distribution were prepared by the micro-contact printing technique (μCP).[30,31] POP stamps were obtained by hot embossing the plastomer at 90 °C onto the wafer for 5 min with a weight of 0.3 kg. An inking pad was made by spin-coating a cleaned coverslip with 200 μl of the still uncured Sylgard mix at 300 rpm for 30 s, which was then cured

by heating it to 150 °C for 1 h. After cooling, 400 µl of the BSA–biotin mix was incubated on the cured Sylgard overnight. The remaining protein solution was dried with an argon stream. The POP stamp was pressed onto the pad with a well defined weight of 0.3 kg for 7 min using a Fineplacer (series 96, Finetech, Berlin, Germany). Stripping the stamp off of the pad and pressing it for 7 min on a cleaned coverslip with the same force transferred the dried protein at the site of the pattern in a controlled manner. The patterned cover-slips, which served as substrates for GUV adhesion, were stored dry at 4–8 °C and used within 3 days.

Prior to the experiment the prepared substrates were placed in a chamber, which was then filled with buffer solution. The remaining regions of bare glass were passivated with 5 mg mL^{-1} BSA for 15 min. Excess protein was removed by exchanging the buffer against protein free PBS in a series of typically ten washing steps. In a second step NAV–TMR was added to the chamber in large excess for 30 min at a final concentration of 100 µg mL^{-1}. After another exchange of buffer, the first passivation step with BSA was repeated and buffer exchanged again.

The specificity of the binding between NAV–TMR and patterned BSA–biotin was checked with fluorescence microscopy. A high intensity marked the NAV–TMR position. This intensity was detected only at BSA–biotin sites, usually exceeding the background signal by a factor 6, indicating highly specific binding. Moreover, fluorescence images served as a control of the pattern quality: any lack of BSA in the first passivation layer became apparent as increased background intensity, since NAV–TMR could bind unspecifically to the substrate. In addition, defects at patterned substrate sites were easily detected from missing fluorescence. A typical fluorescence image of bound NAV–TMR is shown in Fig. 2A.

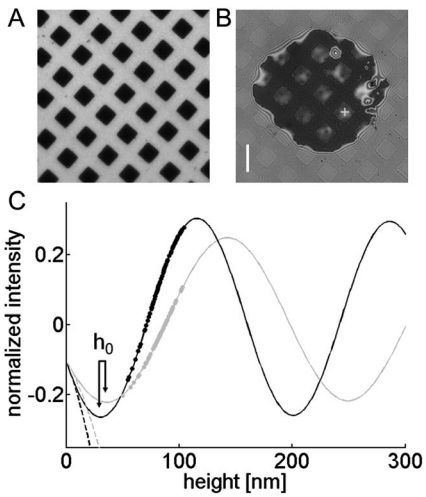

Fig. 2 (A) Fluorescence image of printed adhesive protein NAV–TMR. (B) RICM micrograph of an adhered vesicle on the large grid structure. (C) DW-RICM theoretical curves relating normalized intensity to height of the membrane above the substrate for $\lambda_g = 546$ nm (grey) and $\lambda_b = 436$ nm (black). Solid lines are valid within fluctuation areas, whereas dashed lines are valid for adhesive sites. Considering three reflecting interfaces, the phase of the cosine relating the intensity to the height, is shifted by an offset h_0. 100 data points collected from the same pixel over time allow for an unambiguous determination of the instantaneous height at each time point (grey and black dots) from considerations of continuity. A white cross (B) marks the point of the collected data displayed in (C). Scale bar for (A) and (B): 7 µm.

Giant unilamellar vesicles (GUVs) consisting of SOPC with 2 mol% DOPE–PEG 2000 and 5 mol% DOPE–cap-biotin were prepared *via* electro-swelling.[32] 20 µL of the lipid dissolved in chloroform (2 mg mL^{-1}) was dispersed on glass slides coated with indium tin oxide (pgo, Iserlohn, Germany) and the solvent removed under vacuum overnight. Two lipid coated glass slides were mounted at a distance of 1 mm in a teflon chamber filled with 230 mOsm l^{-1} sucrose solution. An alternating voltage of 1.7 V and 10 Hz was applied for 1.5 h. This yielded giant unilamellar vesicles of about 35 µm average diameter. The vesicle solution was stored at 4–8 °C and used for at most 2 days. For experiments, vesicles were immersed in a PBS buffer of 300 mOsm l^{-1} (unless stated otherwise). Osmolarities were measured before each experiment with an osmometer (Osmomat 030, Gonotec GmbH, Berlin, Germany). The refractive indices of the vesicle solution, n_{in}, and the outer buffer, n_{out}, were measured for each experiment with an Abbe Refractometer (AR4D, Krüss, Hamburg, Germany).

20 µL of the vesicle solution was added to the experimental chamber. Observation chambers completely filled with PBS buffer (volume 1 mL) were covered with a glass slide to avoid osmolarity changes due to evaporation. For measuring static adhesion, measurements were started after more than 30 min, when a final vesicle adhesion state was reached. To monitor dynamic changes, measurements were started after the vesicle adhered for more than 30 min and subsequently buffer osmolarities were altered.

The complete model system and its molecular components are illustrated in Fig. 1.

Image acquisition

Images were acquired with a DW-RICM setup described in detailed before.[33] An inverted microscope (Zeiss Axiovert 200, Carl Zeiss, Göttingen, Germany) equipped with a filter cube with crossed polarizers and a 63× Antiflex Plan-Neofluar oil objective with a numerical aperture of 1.25 and built in lambda quarter plate was used. Light emitted by a metal halogenide lamp (X-Cite, Exfo, Quebec, Canada) was filtered using a dual-interference filter ($\lambda_g = 546 \pm 10$ nm and $\lambda_b = 436 \pm 20$ nm). The numerical aperture of illumination was set to 0.54. In order to achieve maximum contrast the antiflex technique was applied.[34] For DW-RICM two micrographs were recorded simultaneously. For this purpose, the reflected light was split according to its wavelength (FT 460 nm, LP 470 nm (Carl Zeiss, Göttingen, Germany) and BP 436 ± 10 nm (AHF, Tübingen, Germany)) and focused on two separate digital CCD cameras (sensicam qe, PCO, Kehlheim, Germany). Image recording was controlled by the software OpenBox (version 1.77, Informationssysteme Schilling, Munich, Germany). One camera was triggered by the other to ensure simultaneous image acquisition. For vesicles in equilibrium, we recorded 2000 consecutive micrographs with a frame rate of 20 Hz. To monitor vesicles during osmotic buffer changes, approximately 200 frames were recorded prior to the disturbance and recording was continued for about 1000 frames. Here, the frame rate was set to 10 Hz.

Data analysis

The adhesion state of the structured adhered vesicles was probed using dual-wavelength reflection interference contrast microscopy (DW-RICM). This technique is based on recording an interference pattern, which forms from the reflection of polarized light at different interfaces within a sample. Interfering light rays lead to intensity variations I at the image plane which correspond directly to the layer spacing in the sample.[11,12] In contrast to conventional RICM, for DW-RICM two interferograms of different wavelengths are recorded simultaneously, which allows one to lift the phase ambiguity in the periodic intensity pattern.[35] Hence, data of two independent interference patterns yield one specific substrate–object spacing. From these micrographs, maps of membrane–substrate distances with 4 nm axial resolution were calculated. Within stamp free regions of the adhesion zone three planar reflecting interfaces, namely, glass–outer buffer, outer buffer–vesicle membrane, vesicle membrane–inner buffer were considered. Within BSA–biotin printed regions the outer buffer layer was exchanged by the protein layer. The intensity distribution was calculated from the effective reflection coefficient R (and its complex conjugate $R^{\dagger}$), according toref. 36:

$$\begin{aligned} &I = R^{\dagger}R\cdot I_0 \text{ where} \\ &R = r_{01} + r_{12}\left(1 - r_{01}^2\right)e^{-ik\Delta_1} + \\ &r_{23}\left(1 - r_{12}^2\right)\left(1 - r_{01}^2\right)e^{-ik(\Delta_1+\Delta_2)} \end{aligned} \quad (1)$$

and

$$r_{ij} = \frac{n_i - n_j}{n_i + n_j},\ k = \frac{2\pi}{\lambda},\ \Delta_i = 2n_i d_i.$$

The refractive indices of the layers, n_i, were: $n_0 = n_{glass} = 1.525$, $n_1 = n_{out} = 1.335$ or $n_1 = n_{protein} = 1.386$,[37] $n_2 = n_{lipid} = 1.486$[11] and $n_3 = n_{in} = 1.3434$. I_0 is the intensity of the illumination light, $\lambda = \lambda_{g/b}$ are the spectral lines at 546 nm and 436 nm, respectively, of the metal halogenide lamp and $d_2 = 4$ nm is the thickness of the vesicle membrane.[38] $d_1 = h$ was the height of the membrane–substrate distance to be determined. Normalizing the effective reflection coefficient R by the contributions from the background[39] B and substituting in eqn (1), synthetic data for the normalized intensity I_{norm} at a given height h were obtained. I_{norm} is defined as follows:

$$I_{norm} = \frac{R^{\dagger}R - B^{\dagger}B}{B^{\dagger}B}. \quad (2)$$

These synthetic data varied as a cosine function, shifted by an offset $h_0 = 35$ nm. From this the sum S and difference D of the maximal and minimal I_{norm} were calculated. Accounting for the divergence of the incident beam a recently established theory of partial coherent imaging states that[16]

$$I(h) = \frac{1}{2}\left(S - D\frac{\sin(y)}{y}\cos\left\{2kn_1\left[h\left(1 - \sin^2\left(\frac{\alpha}{2}\right)\right) - h_0\right]\right\}\right). \quad (3)$$

Here, $y = 2kh\sin^2\left(\frac{\alpha}{2}\right)$ and α is the half angle of the cone of illumination. Fig. 2C shows the theoretical curves of the normalized intensity I *versus* height h for λ_g and λ_b accounting for finite illumination numerical aperture. Next to the theoretical curves of fluctuating regions (solid lines), $I(h)$ for the stamped regions (dashed lines) is shown at small h. To obtain maps of membrane–substrate distances from the measured interferograms, the entire image (the vesicle as well as the background) was first corrected for anomalies arising from an inhomogeneous illumination.[33] Next, the average background intensity in the image I_{bk} was measured and the entire image was normalized with respect to I_{bk}. Finally, the normalized intensities were used in eqn (3) as $I(h)$, from which the corresponding membrane–substrate distance was calculated. Due to the periodicity of the cosine function in $I(h)$ the correct branch for conversion was determined uniquely, solely by the analysis of two simultaneously recorded interferograms. Fig. 2C gives an example of the intensity data for the two colours exhibiting a high correspondence in height for one particular branch. The oscillating functions of both spectral wavelengths $I(h)$ exhibit a combined periodicity of 816 nm, which defines the upper limit of unambiguous height determination.

All the analysis was done using routines written in Matlab (R2010b, The MathWorks Inc., MA, USA). Automated, time-resolved reconstruction of membrane conformation as well as treatment of shot noise afflicted images was performed as published before.[33]

3 Results and discussion

3.1 Mapping of membrane shape

GUVs doped with biotinylated lipids were allowed to sediment onto receptor patterned substrates and adhered within a few minutes. The membrane–substrate contact zone exhibited bound and fluctuating membrane areas in accordance with the underlying pattern (see Fig. 2B). In RICM this was visible as dark structures at adhesive NAV–TMR receptor sites where the membrane was bound to the substrate. In the passivated neutral or non-adhesive pockets, strong intensity variation in RICM indicated a freely fluctuating membrane.

The specificity of vesicle binding to NAV–TMR patterned substrates was quantified using either vesicles without biotinylated lipids or substrates without NAV–TMR. Most of the vesicles, (80% and 86%, respectively) did not adhere, while the others exhibited either pinning sites or partial adhesion. In addition, unlabelled neutravidin was used instead of NAV–TMR, to exclude any unspecific adhesion effects of the fluorophore. Here, no changes in the recorded adhesion state were detected. Membrane topography in the adhering zone as well as in the fluctuating pockets was analysed using DW-RICM.[33] An osmotic pressure difference of 70 mOsm l^{-1} (230 mOsm l^{-1} sucrose inside the vesicle and 300 mOsm l^{-1} PBS buffer outside of the vesicle) was chosen for in-depth characterization of the membrane shape and fluctuations. Fig. 3A gives typical examples of structured adhered vesicles on the large grid, the small grid and the line structure, respectively. In each case, the membrane was attached to the receptors on the adhesive grid at a fixed average height of 19 ± 5 nm (161 adhesion areas were analysed),[40] as determined from DW-RICM topography reconstruction. In addition, atomic force microscopy analysis of each substrate preparation step resulted in a total average height of

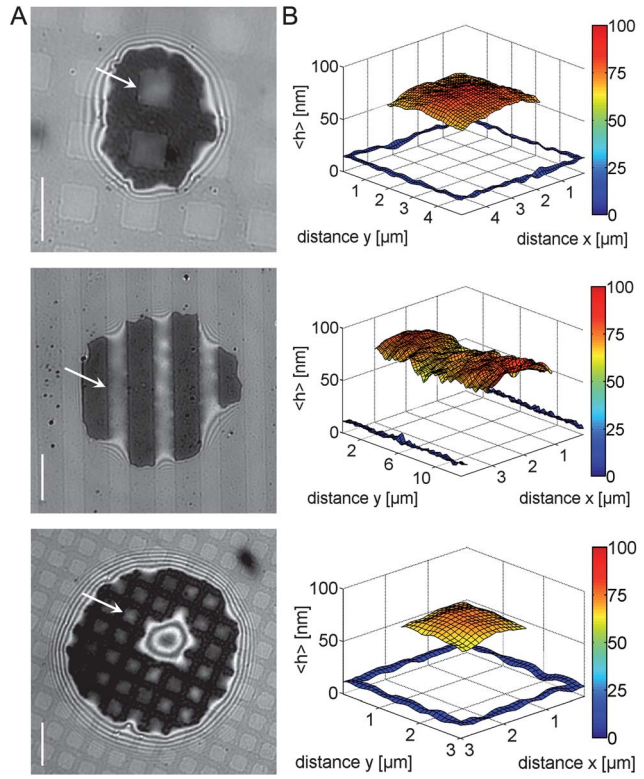

Fig. 3 (A) RICM micrographs of vesicles adhering to the large grid structure (top), line structure (middle) and small grid structure (bottom). Scale bar: 7 µm. (B) Reconstruction of the average membrane topography within the fluctuation area marked with a white arrow in (A). Only the quasi-flat parts of the membrane, corresponding to the adhered edge at about 20 nm and the fluctuating plateau, are shown. The highly inclined and/or curved part of the membrane connecting the edge and the plateau is not shown. The colour coding indicates average heights in nm.

20 nm: 13 ± 5 nm (10 substrates) was measured for the BSA–biotin patterned layer alone and a 7 ± 1 nm height increase was measured after NAV–TMR binding to the BSA–biotin (data not shown).

Within the passivated zones corresponding to areas of fluctuating membrane, a finite separation between the membrane and the substrate, henceforth referred to as the local membrane height h at a specific time, was maintained. Height reconstruction within these fluctuating regions revealed that the membrane rises sharply from the patterned edge of each pocket within ~0.5 µm and forms a plateau around the center. The transient region at the edge should be comparable to the persistence length, and this region agrees well with the persistence length of 0.7 µm determined for a similar system.[11] The central plateau was 1.6^2 µm^2 in size for the small, 3.0^2 µm^2 for the large and 2.0 µm wide for the line structure. The height analysis used here (see eqn (3)) is applicable only to the quasi-flat fluctuating and bound regions. Furthermore, the boundary between the stamped and passivated regions appeared rough in the micrographs. Therefore, to avoid errors, seven pixels around the fluctuation area were left out in the reconstruction (see Fig. 3B).

In the following, nine neighbouring points in the centre of each fluctuation area were considered (see *e.g.* the position of the white cross in Fig. 2) and the height values over time of each were extracted. These were plotted in a histogram and fitted with a normal distribution to verify the applicability of Gaussian statistics. Heights were averaged over time and, subsequently, the average of the nine mean heights and standard deviations was calculated. Analyzing 88 exemplary fluctuation areas of the large grid structure yielded $\langle h \rangle = 76 \pm 8$ nm (see section 3.3.2 for average height values to other osmotic gradients). The average of 80 fluctuation areas of the small grid structure and 27 areas of the line structure resulted in $\langle h \rangle = 81 \pm 9$ nm and $\langle h \rangle = 82 \pm 8$ nm, respectively. Thus, the average membrane–substrate distance within the fluctuation regions was independent of the underlying structure. Long term studies of fluctuation areas over 30–60 min revealed no significant changes.

3.2 Mapping of membrane fluctuations

The membrane–substrate distance was mapped for each frame in a sequence of DW-RICM movies. For the determination of the mean square fluctuation amplitudes, squared deviations from the mean height were averaged over time $\langle \delta h^2 \rangle = \langle (h(t) - \langle h \rangle)^2 \rangle$ for each of the nine central pixels. Then, the root value was averaged over all pixels, resulting in fluctuation amplitudes of 12 ± 2 nm on the large grid structure, 9 ± 3 nm on the small grid structure and 9 ± 4 nm on the line structure. Amplitude values for the three structures were also found to be the same within the statistical error. Table 1 gives an overview of the average heights and fluctuation amplitudes obtained. Interestingly, for this particular range of shapes and sizes we do not see any impact from the pattern on the average height and fluctuation amplitudes.

These values are in good agreement with fluctuations reported earlier[15,20,22] in studies on vesicles in the adhesion process. Similar amplitudes were also found by Rädler and Sackmann,[11] who observed unspecifically adhered vesicles.

For further characterization, the two-dimensional spatial spectrum of the membrane out-of-plane fluctuations was derived. It was first checked that the recorded image sequences were long enough to yield sufficient uncorrelated data—an essential prerequisite of Fourier analysis. If this were not the case, the measured equilibrium values could be influenced by fluctuations with long relaxation times giving erroneous results. In order to test this, first the relaxation of the longest wavelength was determined. Average membrane profiles over an increasing number of images were calculated and these subtracted from each other. At a recording time of ~5 s, corresponding to 100 images in our case, hardly any detectable change between the profiles existed and the difference image was close to zero (data not shown). This indicated one set of uncorrelated data, where the longest wavelength had relaxed. Thus, from recording 2000 images, 20 sets of uncorrelated data were obtained. An extension of recording times to > 3000 images was not feasible, due to focus drift.

Table 1 An overview of the average heights and fluctuation amplitudes on different adhesion structures. # Denotes the number of evaluated fluctuation areas. The presented errors refer to the standard deviation of the population

Structure	Large grid	#	Small grid	#	Line	#
$\langle h \rangle$ [nm]	76 ± 8	88	81 ± 9	80	82 ± 8	27
$\sqrt{\langle \delta h^2 \rangle}$ [nm]	12 ± 2	54	9 ± 3	80	9 ± 4	27

Fast Fourier transformation (FFT) maps were calculated from amplitude maps $A(m,n,t) = h(m,n,t) - \langle h(m,n)\rangle_t$ for each time point according to:

$$A(k,l,t) = \frac{1}{N^2}\sum_{m=0}^{N-1}\sum_{n=0}^{N-1} A(m,n,t)e^{-i\frac{2\pi mk}{N}}e^{-i\frac{2\pi nl}{N}},$$

where $N \times N$ are the number of pixels within the fluctuation region, indexed (m,n). Fourier amplitudes $A(k,l,t)$ were then averaged over the whole time sequence, TS, according to $\langle A^2(k,l)\rangle = \frac{1}{TS}\sum_{t=1}^{TS} A^2(k,l,t)$. Examples of mean square amplitude maps in Fourier space are depicted in Fig. 4B. These Fourier maps exhibit regions of approximate radial (for the grids) and axial (for the lines) symmetry in the dominating wave vectors. The theoretical fourfold symmetry of small and large grid structure was exploited to radially project the 2D spectrum onto the wave vector

$$q = \sqrt{q_x^2 + q_y^2} = \sqrt{\left(\frac{n\pi}{L_x}\right)^2 + \left(\frac{m\pi}{L_y}\right)^2}.$$

Here, the first equality is the vector norm and the second equality defines the eigenmodes of the wave equation. $q_{x,y}$ is the wave vector along one axis and $L_{x,y}$ the side length of the fluctuation area. In the case of the line structures only $q = q_y$ along the long axis was evaluated (see Fig. 4C).

Plotting these projections for the large grid structure, one distinct wave vector at $q = 1.64 \pm 0.13$ μm^{-1} and another less dominant wave vector at $q = 1.15 \pm 0.13$ μm^{-1} were found. A comparison of these values to theoretically expected modes[41] for fluctuations of a square area $L^2 = 4.2 \times 4.2$ μm^2 resulted in a good agreement with the (2,1) mode, the so called 'swapping mode', for the predominant wave vector. Corresponding wavelengths for the two spatial directions were $\lambda = 4$ and 8 μm. The second contributing wave vector corresponded well with the (1,1) mode, the so called 'breathing mode', of $\lambda = 4$ μm length. For the small grid structure only one wave vector at $q = 2.4 \pm 0.2$ μm^{-1} and $\lambda = 4$ μm primarily developed. This value corresponded to the 'breathing mode'. Interestingly, we find that the first mode which requires a change in the volume trapped in the pockets is seen in both, the small and large grid, while for the large grid an additional mode, which conserves the volume, dominates the spectrum more often. We conclude, that this may arise from some limitation in the permissible volume change.

Finally, analysis of line structures yielded contributions of several modes. From each spectrum only the predominant mode was considered. Most often the first mode was predominant, with an average ratio of wavelength/adhered length of $\lambda_y/L_y = 1.94 \pm 0.81$. The sixth mode, with $\lambda_y/L_y = 0.31 \pm 0.06$, dominated less often. The second and fourth modes, with $\lambda_y/L_y = 1.00 \pm 0.30$ and $\lambda_y/L_y = 0.50 \pm 0.15$, respectively, contributed most to the spectrum in some cases. Note, that due to the highly variable length of the linear fluctuation area, different wavelengths could

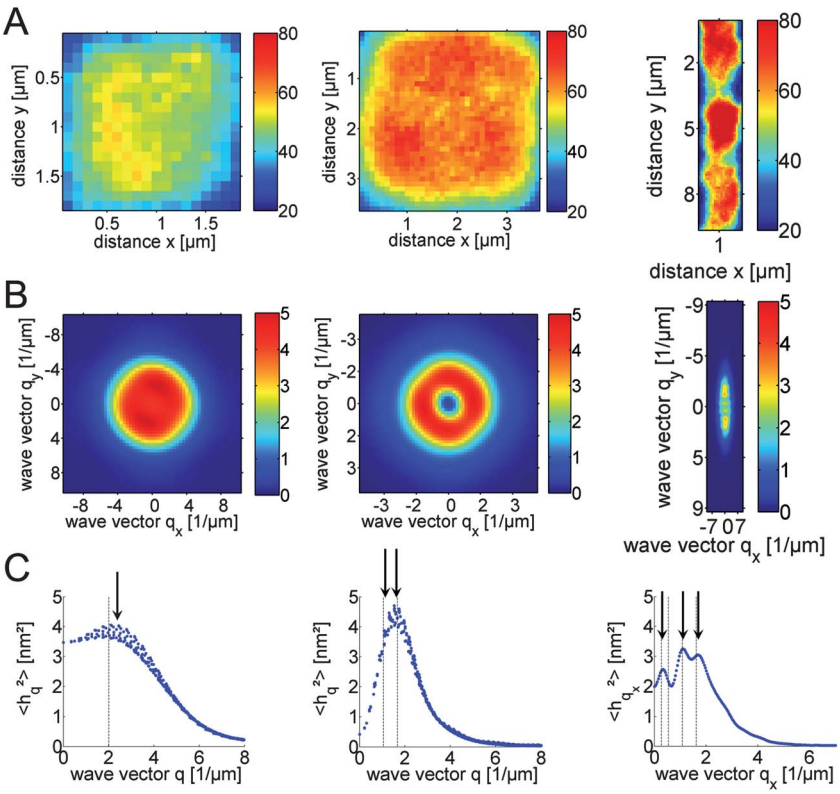

Fig. 4 Examples of FFT analysis on a small grid structure (left), a large grid structure (middle) and a line structure (right). (A) Mean square amplitude maps in nm^2. (B) Fourier maps in nm^2. (C) Radial average of Fourier maps (large grid and small grid structures) and the fluctuation spectrum along the y-axis (line structure). Black arrows and dashed lines indicate the position of the observed average wave-vectors and corresponding theoretical values, respectively. In the case of a line, values for the specific example are shown, as line lengths vary.

correspond to one specific mode, which explains the large statistical spread in wavelengths.

Theoretically, fluctuations of a membrane pinned to a quadratic array were studied by Merath and Seifert.[42] They found maxima in shape fluctuation spectra at wavelengths corresponding to twice the tethering distance. In part this result is also seen in the present analysis, as the first mode of each structure always contributes. Table 2 gives an overview of the statistics to this analysis.

3.3 Influence of membrane tension on fluctuations and height

Since in this system the membrane tension is determined by the osmotic difference between the outside and the inside of the vesicle, the tension can be changed by changing the initial osmolarity of the outer and inner buffer. We took advantage of this to study the influence of membrane tension on the shape of the constrained membrane and the fluctuations.

3.3.1 Osmotic shock. In order to study the evolution of membrane fluctuation and height under a strong osmotic pressure difference we administered osmotic shocks. The behaviour of the vesicle on the large grid and small grid structures turned out to be equivalent, and the results reported below are representative of both. Fig. 5 illustrates the reaction of structured adhered vesicles to osmotic deflation, corresponding to a tension decrease. Shortly after the addition of PBS increasing the osmotic strength of the outer buffer (~5 s after addition), an increase in the membrane–substrate distance within the fluctuating regions was observed. Often, a distance of several hundred nanometres was reached within a few minutes. 15–30 min later the average height decreased, usually to about one third of its maximal value (data not shown).

In a second set of experiments the reverse disturbance, namely, osmotic inflation and consequently a vesicle tension increase, was monitored (see ESI†). Water was added to the chamber and, instantaneously, membrane heights within the fluctuation areas decreased. Within a minute, membrane heights reached the substrate, and membrane fluctuations were not detected anymore. Corresponding to osmotic deflation experiments, a partial recurrence of membrane fluctuations and elevated membrane heights was observed.

Table 2 Experimental results of FFT analysis for the small grid, the large grid and the line structure. Predominant modes, average wavelengths λ and corresponding average sidelengths $L_{x/y}$ are given. # Denotes the number of evaluated regions where this mode was predominant. The other contributing modes of each spectrum were not considered in the statistics. Note that line structures exhibited a highly variable length L_y, wherefore the statistical spread is higher

Small grid	Mode	λ[μm]	$L_{x/y}$[μm]	#
	(1,1)	4	2.0 ± 0.2	43
Large grid	Mode	λ[μm]	$L_{x/y}$[μm]	#
	(1,1)	8	4.2 ± 0.2	6
	(1,2)	4	4.2 ± 0.2	65
Line	Mode	λ_y[μm]	L_y[μm]	#
	1st	33 ± 14	17 ± 7	13
	2nd	7 ± 2	7 ± 2	5
	4th	7 ± 2	14 ± 4	4
	6th	5 ± 1	16 ± 4	7

Both observations can be explained by the initial incomplete mixing of solutes in the chamber (sugar molecules, ions, *etc.*), which causes a fast and strong variation in vesicle membrane height. This is then followed by the relaxation to equilibrium, where solutes are evenly distributed and where the membrane height slowly adjusts to the final concentration.

These observations have two important implications: first, the membrane is fluid within the adhesion zone, allowing for lipid exchange between adhered and fluctuation regions (which was also verified by FRAP (fluorescence recovery after photobleaching)[33]). Second, it appears energetically favourable to increase the membrane–substrate distance with decreasing tension and *vice versa*.

3.3.2 Preimposed osmotic pressure difference. As described above, the behaviour under osmotic shock is complex. In order to avoid misinterpretation of the data due to the abrupt osmotic pressure change, we also studied vesicles exposed to an initial osmotic pressure difference of $\Delta\Pi$ = 20, 70, 120, 145 or 170 mOsm l^{-1}. Fig. 6A gives an overview of the monitored states after adhesion was completed.

We observed that with increasing initial osmotic pressure difference, the average membrane height within the fluctuation regions rises. At $\Delta\Pi$ = 20 mOsm l^{-1}, fluctuations were suppressed and the membrane appeared to be adhered. With an increase of $\Delta\Pi$ to 70 mOsm l^{-1}, the membrane resided at average heights further away from the substrate and fluctuations were clearly visible. Increasing the osmotic gradient even further, not only were higher equilibrium heights and stronger fluctuations detected, but also a trend to larger adhesion zones was observed. This effect is attributed to a larger excess area of the vesicle, which results from high osmotic deflation, which in turn corresponds to a low membrane tension. The measured ratio 'vesicle radius/contact area radius' R_V/R_A, which will later be shown to be decisive in determining the contribution to the membrane–substrate interaction from gravity, is 2.1, 1.7, 1.5, 1.1 and 1.0 in order of increasing $\Delta\Pi$. Measurements at even higher osmotic gradients were not feasible as the vesicles started to bud.

Quantitative results on vesicle adhesion at different osmotic gradients, or, equivalently, membrane tensions, are given in Fig. 6B and C. Depending on the initial gradient, average membrane heights vary between 0 and ~550 nm. Between $\Delta\Pi$ = 70 and 120 mOsm l^{-1} a strong increase in average heights is observed, the increase becomes less pronounced at higher osmotic gradients. There are two possible reasons for this observation, which may contribute at the same time, (a) at high osmotic gradients vesicles are unstable and may loose excess area from budding already during sedimentation,[43] thus increasing the tension above the expected value, or (b) the increasing weight of the vesicle compensates for the decrease in tension.

Mean square fluctuation amplitudes (see Fig. 6C) exhibited a similar trend to the measured average heights: an initially strong increase of 36 nm^2—which denotes the base value due to shot noise—to 300 nm^2 is followed by a leveling off at high osmotic gradients.

3.3.3 Data interpretation in light of the membrane–substrate interaction. From the above observations of (1) the formation of a height plateau, (2) the equal average membrane height within

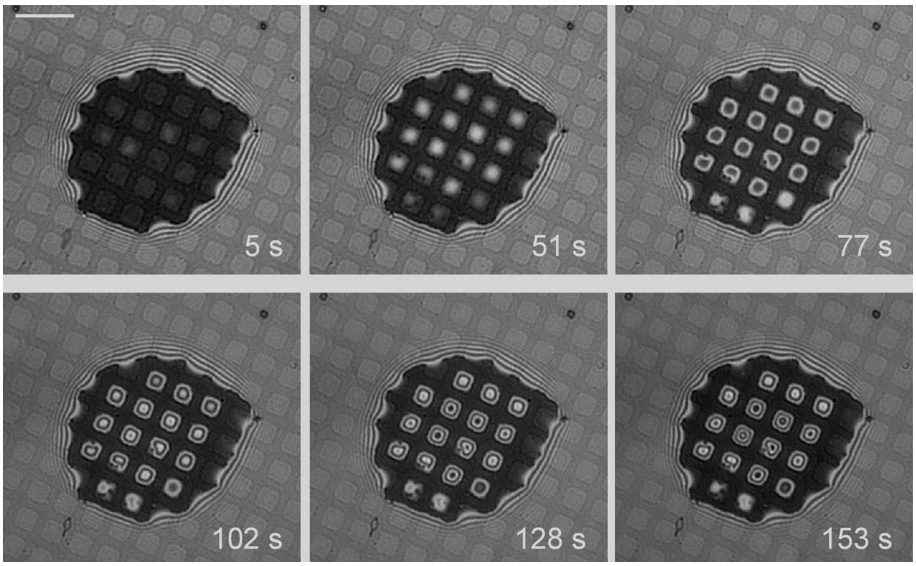

Fig. 5 RICM micrographs of a vesicle adhering to the small grid structure undergoing osmotic deflation which drives the vesicle membrane upwards. Scale bar: 7 μm.

fluctuation regions for all the structures, (3) the fluctuation amplitude being independent of the underlying structure, and (4) the verification of lipid mobility within the bound parts, we interpret the membrane shape as being in equilibrium, in which the membrane in the flat region of the plateau in fact resides at the minimum of an unspecific interaction potential.

The membrane–substrate interaction can be written as a simple superposition of unspecific interaction terms.[15,44] Contributing interactions are the entropic Helfrich repulsion, V_H, which arises from thermally induced membrane fluctuations, the polymer steric repulsion, V_{rep}, at very short distances of the membrane from the substrate, the attractive van der Waals interaction, V_{vdW}, and gravity, V_{grav}. The parameters appearing in these equations can be either directly measured (henceforth indicated by M), calculated for the given experimental setting, (C), or they are available from the literature, (L). The vesicle tension σ can not however be directly measured.[16] In the following we consider each term of the interaction potential.

The Helfrich interaction for a vesicle membrane with tension σ and a dimensionless prefactor b, determined to be $b \sim 0.1$ (L), as introduced by Seifert[7]

$$V_H(h_s) = \frac{1.5bk_BT\sigma}{\kappa sinh^2\left(\frac{h_s}{2}\sqrt{\frac{\sigma}{bk_BT}}\right)}. \quad (4)$$

$h_s = h - R_{BSA} - R_{PEG}$ is the glass–membrane distance shifted by the radii of gyration of BSA, $R_{BSA} = 4.5 \times 10^{-9}$ m (L),[45] and PEG, $R_{PEG} = 3.4 \times 10^{-9}$ m (L),[46] since the adsorbed protein on

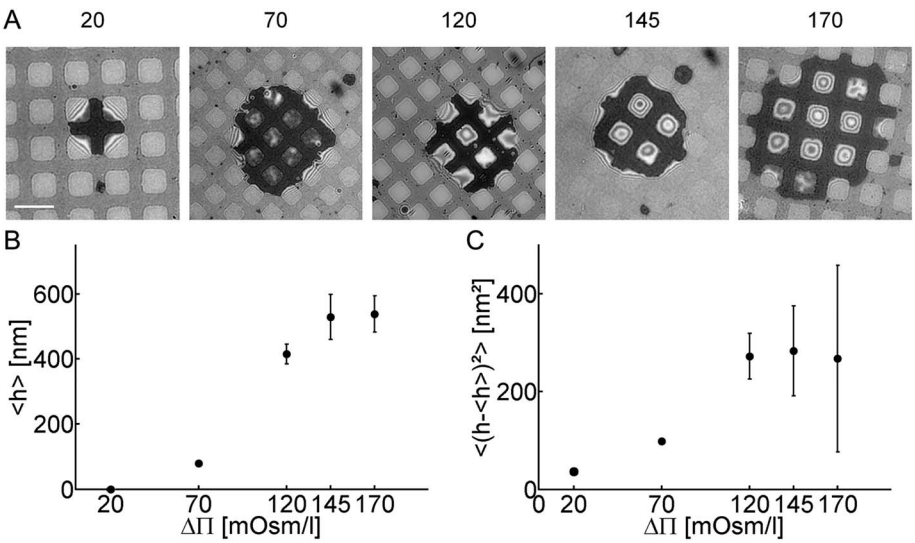

Fig. 6 (A) RICM micrographs of vesicles adhering to the large grid structure. An increase in the initially imposed osmotic pressure difference results in an increase in the equilibrium height (left to right): $\Delta\Pi = 20$, 70, 120, 145 and 170 mOsm l^{-1}. Scale bar: 7 μm. (B) Average membrane heights $\langle h \rangle$ within the fluctuation regions rise from 0–550 nm. (C) Mean square fluctuation amplitudes $\langle (h) - \langle h \rangle^2 \rangle$ increased from 36 nm^2, which marks the base value due to shot noise, to 300 nm^2.

the substrate and the polymer bound to the vesicle membrane prevent the membrane from probing smaller heights. $\kappa = 20\ k_BT$ (L) is the bending rigidity for SOPC[47] with k_B (L) the Boltzmann constant and $T = 293$ K (M) the temperature.

Polymer steric repulsion was calculated according to Bruinsma *et al.*:[15]

$$V_{rep}(h_s) = \frac{\pi^2}{6} k_B T \rho_{PEG} \left(\frac{R_{PEG}}{h_s}\right)^2 e^{-\frac{3}{2}\left(\frac{h_s}{R_{PEG}}\right)^2}, \quad (5)$$

where $\rho_{PEG} = 3.6 \times 10^{16}$ 1/m^2 (C) is the density of pegylated lipids in the vesicle.

The van der Waals (vdW) interaction was determined for the four layer system, glass (g)—buffer (b)—membrane (m)—sucrose solution (s), as given by Parsegian:[48]

$$V_{vdW}(h_s) = -\frac{A_{gb|mb}}{12\pi}\left(\frac{1}{h_s^2} - \frac{1}{(h_s + d)^2}\right). \quad (6)$$

$d = 4 \times 10^{-9}$ m (L) is the thickness of the bilayer[38] and $A_{gb|mb} = 7 \times 10^{-21}$ J (C) the Hamaker constant, determined from Lifshitz theory. This is in good agreement with the Hamaker constants usually found for biological material immersed in water (1–4 k_BT).[44,49]

Gravity is given by:

$$V_{grav}(h_s) = \frac{V}{A} \cdot \Delta\rho \cdot g \cdot h_s, \quad (7)$$

with $V = 4/3\pi R_V^3$ (M), the vesicle volume, $\Delta\rho$ (C), the density difference between vesicle interior and exterior, and g (L), the acceleration due to gravity. $A = \pi R_A^2$ (M) is the contact area of the vesicle and the measured ratio R_V/R_A was used as mentioned in section 3.3.2. Applying these values and van't Hoff's equation[50] $\Delta\rho = 0.02, 0.03, 0.05, 0.06, 0.07$ g cm^{-3} for increasing $\Delta\Pi$, was calculated.

To compare with our data, the resulting interaction potential $V_T = V_H + V_{rep} + V_{vdW} + V_{grav}$ was calculated, with the tension σ as a free parameter which was varied in reasonable limits.[51] However, the minima of these effective interaction potential curves could not be matched to the experimentally determined values. Similar discrepancies between theory and experiment have been observed before.[44,52] We then treated the Helfrich parameter b also as a free parameter. In fact, so far this value has not been measured for a single membrane in a potential. Good agreement for the five sets of experiments was simultaneously achieved using $b = 0.76$ and $\sigma = 500, 50, 0.1, 0.1$ and 0.1 μJ m^{-2} for increasing $\Delta\Pi$. A similarly high Helfrich parameter of $b = 0.56$ was derived by Netz[53] in a theoretical calculation for the one dimensional case of strings and in the limit of a vanishing external potential.

Fig. 7 illustrates the interaction potential curves V_T obtained from these values for the different osmotic gradients. Their trends and the particular form of the above terms demonstrate several general aspects:

First, a strong decrease in membrane tension results in a large shift of the unspecific minimum towards higher heights. This trend is confirmed by the measured average height. In addition, the minimum of the interaction potential changes from strongly curved at low osmotic differences to a shallow minimum at high osmotic gradients. These changes are also reflected in the

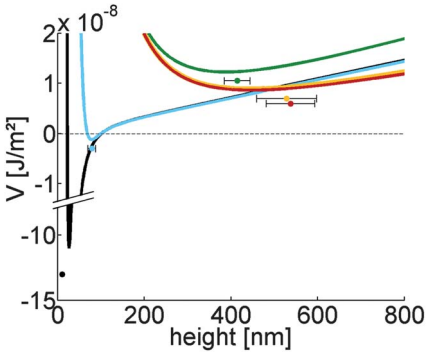

Fig. 7 Effective interaction potential curves calculated for initial osmotic pressure differences of 20 mOsm l^{-1} (black), 70 mOsm l^{-1} (blue), 120 mOsm l^{-1} (green), 145 mOsm l^{-1} (yellow) and 170 mOsm l^{-1} (red). These were calculated according to eqn (4)–(7) with parameters specified in the text, treating the tension as a variable to obtain the best match to the experimentally determined average membrane height (indicated by filled circles with error bars). Note that the data points are the same as those depicted in Fig. 6B.

measured fluctuation amplitudes in Fig. 6C. Moreover, an increase in amplitudes at low osmotic differences should correspond to a tension decrease, and *vice versa*. In the calculation of V_T, the vesicle tension was varied accordingly. However, at high osmotic gradients, the recorded fluctuation was weaker than expected. This discrepancy may arise from the finite resolution of the detector.[44,52]

Second, the van der Waals interaction V_{vdW} has a strong effect on equilibrium heights close to the substrate, while far away from the substrate the effective interaction potential is independent of V_{vdW}.

Third, for high initial osmotic gradients, the shape of the potential is determined mainly by the Helfrich repulsion and gravity. Here, a slight increase in average heights for similar vesicle tensions is observed. It could be expected that during osmotic deflation, the density of the sucrose solution inside the vesicle rises and gravity should contribute slightly more to the membrane–substrate interaction. In this case, equilibrium heights would be shifted to lower values. However, gravity is also governed by the vesicle volume V/contact area A ratio (see eqn (7)), which decreases with osmotic deflation. This dependence counteracts the increase in the density of the sucrose solution and results in a non-trivial dependence of the interaction potential on gravity.

Finally, we examine whether the interior of the GUVs reaches osmotic equilibrium with the outside buffer before adhesion begins. Since it is known that the membrane is permeable to water, but not to ions, the decrease in the vesicle volume can be derived from the known initial sucrose concentration and the measured radius of the adhered vesicles. For the latter, the equatorial vesicle radius, obtained from phase contrast images, together with the adhered vesicle area yielded the radius of the free vesicle. We use this in the equation for the deflation rate[38] and conclude that the equilibration time is ~2 and 1 min for the least and highest osmotic difference, respectively. The sedimentation time for the former and latter case was estimated to be ~3 and 0.5 min(s). Hence, the spread in the measured average height seen in Fig. 6B and C for high initial osmotic difference may be

due to the fact that some of the vesicles continue to equilibrate during adhesion.

4 Conclusion

It is well known that the osmotic deflation of GUVs should lead to a decrease in the membrane tension and hence an increase in fluctuations. However, a quantitative experimental study of this link was not available so far. Our model system, where membranes were partially adhered to a printed micro-pattern, enabled a systematic quantitative study of this link in the context of partially adhered vesicles close to a wall. Here, an underlying chemical micro-pattern divides the membrane into different pockets of fluctuation zones, separated by bands of specifically adhered membrane. Interestingly, the adhered part of the membrane remains fluid and allows not only the exchange of lipids but also a change in the area of the membrane in each fluctuation area. Furthermore, since the membrane is permeable to water, the volume in the pockets is not conserved either.

In each pocket, the membrane assumes a characteristic plateau shape whose height depends on the imposed osmotic deflation, as do the membrane fluctuations in the flat part of the plateau. As could be expected, the spatial modes, that became accessible by Fourier analysis of the membrane shape, do depend on the underlying adhesive structure and reflect its symmetry. Interestingly, a contribution of the first mode—the so called breathing mode that requires a change in the volume trapped in the pocket—is seen in the small and, less dominantly, in the large grids, while on the large grid a predominant contribution of the (2,1) mode is observed. This may indicate a limit to the permissible volume change. In case of lines, the modes develop parallel to the line and depending on the vesicle size, different modes are picked up.

Average height and fluctuation amplitudes in the flat plateau were independent of the underlying geometry. Yet, for a higher variation of receptor concentration/unit area a stronger effect on membrane properties is expected. The dependence of the average height and fluctuation amplitudes in the flat plateau on osmotic deflation, *via* tension, can be interpreted in the light of a relatively simple substrate to membrane interaction potential which does not depend on the size or shape of the printed micro-pattern. The full quantitative comparison with theory is not possible at this stage because the theoretical expression for the Helfrich repulsion relies on a dimensionless parameter "b" which is not independently measurable. Another source of discrepancy, which becomes apparent when the expected and measured fluctuations are compared, is the finite space and time resolution of the camera. Nevertheless, a very good qualitative agreement is seen and the trends observed in the data can be perfectly explained.

The experiments and analysis presented here extend the work of Rawicz *et al.*[38] on osmotic deflation of vesicles to the case of partial adhesion. This case is highly relevant for organs like the kidneys or oesophagus where cells, adhering to each other to form the tissue mass, are subjected to high osmotic pressure differences. By adapting a model system with a well defined adhesion geometry and improving data analysis with DW-RICM, we were able to link increased osmotic deflation with increased membrane fluctuations *via* a tension dependent effective interaction potential.

Acknowledgements

We benefited highly from discussions with Ana-Sunčana Smith, Udo Seifert and Daniel Schmidt. We thank Dr Norbert Kirchgessner and Sebastian Houben for helpful discussions on Matlab and Nico Hampe for the fabrication of microstructured SiO_2 wafers. One of the authors (C. M.) is grateful for the financial support from the Bonn-Cologne Graduate School and the Université franco-allemande.

Notes and references

1 R. J. V. Pulvertaft, *J. Clin. Pathol.*, 1949, **2**, 281–283.
2 R. Blowers, E. M. Clarkson and M. Maizels, *Journal of Physiology*, 1951, **113**, 228–239.
3 F. Brochard-Wyart and J.-F. Lennon, *J. Phys.*, 1975, **36**, 1035–1047.
4 Y. Park, C. A. Best, T. Auth, N. S. Gov, S. Safran, G. Popescu, S. Suresh and M. S. Feld, *Proceedings of the National Academy of Sciences*, 2009, **26**, 1289–1294.
5 W. Helfrich, *Zeitschrift für Naturforschung, Teil C*, 1973, **28**, 693–703.
6 R. Lipowsky and E. Sackmann, *Structure and Dynamics of Membranes*, North Holland, Amsterdam, 1995, vol. I and II.
7 U. Seifert, *Adv. Phys.*, 1997, **46**, 13–137.
8 T. R. Weikl and R. Lipowsky, *Langmuir*, 2000, **16**, 9338–9346.
9 H.-G. Döbereiner, E. Evans, M. Kraus, U. Seifert and M. Wortis, *Phys. Rev. E: Stat. Phys., Plasmas, Fluids, Relat. Interdiscip. Top.*, 1997, **55**, 4458–4474.
10 G. Popescu, Y. Park, R. R. Dasari, K. Badizadegan and M. S. Feld, *Phys. Rev. E: Stat., Nonlinear, Soft Matter Phys.*, 2007, **76**, 031902.
11 J. Rädler and E. Sackmann, *J. Phys.*, 1993, **3**, 727–748.
12 L. Limozin and K. Sengupta, *Biophys. J.*, 2007, **93**, 3300–3313.
13 A. Lambacher and P. Fromherz, *Appl. Phys. A: Mater. Sci. Process.*, 1996, **63**, 207–216.
14 S. Marx, J. Schilling, E. Sackmann and R. Bruinsma, *Phys. Rev. Lett.*, 2002, **88**, 138102.
15 R. Bruinsma, A. Behrisch and E. Sackmann, *Phys. Rev. E: Stat. Phys., Plasmas, Fluids, Relat. Interdiscip. Top.*, 2000, **61**, 4253–4267.
16 K. Sengupta and L. Limozin, *Phys. Rev. Lett.*, 2010, **104**, 088101.
17 L. C.-L. Lin, J. T. Groves and L. H. Brown, *Biophys. J.*, 2006, **91**, 3600–3606.
18 A. Zidovska and E. Sackmann, *Phys. Rev. Lett.*, 2006, **96**, 048103.
19 A. Pierres, A.-M. Benoliel, D. Touchard and P. Bongrand, *Biophys. J.*, 2008, **94**, 4114–4122.
20 A. Albersdörfer, T. Feder and E. Sackmann, *Biophys. J.*, 1997, **73**, 245–57.
21 A.-S. Smith, S.-F. Fenz and K. Sengupta, *Europhys. Lett.*, 2010, **89**, 28003.
22 S. F. Fenz, T. Bihr, R. Merkel, U. Seifert, K. Sengupta and A.-S. Smith, *Adv. Mater.*, 2011, **23**, 2622–2626.
23 M. Mrksich, *Chem. Soc. Rev.*, 2000, **29**, 267–273.
24 D. Cuvelier, O. Rossier, P. Bassereau and P. Nassoy, *Eur. Biophys. J.*, 2003, **32**, 342–354.
25 A.-L. Bernard, M.-A. Guedeau-Boudeville, O. Sandre, S. Palacin, J.-M. di Meglio and L. Jullien, *Langmuir*, 2000, **16**, 6801–6808.
26 D. C. Gerhardt, t. J. Shuck and R. A. Bordeaux, *Gastroenterology*, 1978, **75**, 268–274.
27 N. H. Garcia, C. R. Ramsey and F. G. Knox, *News in Physiological Sciences*, 1998, **13**, 38–43.
28 J. A. Schafer, W. B. Reeves and T. E. Andreoli, *Mechanisms of fluid transport across renal tubules*, Comprehensive Physiology, 2011, 659–713.
29 C. M. Cesa, N. Kirchgessner, D. Mayer, U. S. Schwarz, B. Hoffmann and R. Merkel, *Rev. Sci. Instrum.*, 2007, **78**, 034301.
30 A. Kumar and G. M. Whitesides, *Appl. Phys. Lett.*, 1993, **63**, 2002–2004.
31 A. P. Quist, E. Pavlovic and S. Oscarsson, *Anal. Bioanal. Chem.*, 2005, **381**, 591–600.
32 D. S. Dimitrov and M. I. Angelova, *Bioelectrochem. Bioenerg.*, 1988, **19**, 323–336.
33 C. Monzel, S. Fenz, R. Merkel and K. Sengupta, *ChemPhysChem*, 2009, **10**, 2828–38.

34 J. S. Ploem, *Mononuclear Phagocytes in Immunity, Infection and Pathology*, Blackwell Scientific, Oxford, 1975.
35 J. Schilling, K. Sengupta, S. Goennenwein, A. R. Bausch and E. Sackmann, *Phys. Rev. E: Stat., Nonlinear, Soft Matter Phys.*, 2004, **69**, 021901.
36 For spatial reasons the $(\lambda,\vec{x})$ dependence of I and R are suppressed.
37 K. Spaeth, A. Brecht and G. Gauglitz, *J. Colloid Interface Sci.*, 1997, **196**, 128–135.
38 W. Rawicz, K. C. Olbrich, T. McIntosh, D. Needham and E. Evans, *Biophys. J.*, 2000, **79**, 328–39.
39 The background B is the theoretically expected reflectivity of the areas in the image plane which are free of the investigated object.
40 The presented errors refer to the standard deviation of the population.
41 For a membrane of area L^2 the wave vector is given by $q_{x,y} = \frac{2\cdot\pi}{\lambda}(k,l)$ with k, l = 0,…, $N-1$ and λ the fluctuation wavelength. As the membrane is bound to the substrate at distinct points, boundary conditions constrain the modes to multiples of half the wavelength $L_{x,y} = n\cdot\frac{\lambda}{2}, n\in N$. Thus, wave vectors become: $q_{x,y} = n\frac{x}{L_{xy}}$.
42 R.-J. Merath and U. Seifert, *Phys. Rev. E: Stat., Nonlinear, Soft Matter Phys.*, 2006, **73**, 010401.
43 A.-L. Bernard, M.-A. Guedeau-Boudeville, L. Jullien and J.-M. di Meglio, *Biochim. Biophys. Acta, Biomembr.*, 2002, **1567**, 1–5.
44 J. O. Rädler, T. J. Feder, H. H. Strey and E. Sackmann, *Phys. Rev. E: Stat. Phys., Plasmas, Fluids, Relat. Interdiscip. Top.*, 1995, **51**, 4526–4536.
45 E. M. Slayter, *J. Mol. Biol.*, 1965, **14**, 443–452.
46 J. Majewski, T. L. Kuhl, M. C. Gerstenberg, J. N. Israelachvili and G. S. J. Smith, *J. Phys. Chem. B*, 1997, **101**, 3122–3129.
47 Y. Zhou and R. M. Raphael, *Biophys. J.*, 2005, **89**, 1789–1801.
48 V. A. Parsegian, *Van der Waals forces: a handbook for biologists, chemists, engineers, and physicists*, Cambridge University Press, Cambridge, 2006, p. 380.
49 J. N. Israelachvili, *Intermolecular and Surface Forces*, Academic Press, Waltham, 3rd edn, 1991.
50 J. W. Gibbs, *Nature*, 1897, **55**, 461–462.
51 The applicable vesicle tension regime was estimated from the scaling behaviour of the fluctuation strength, $\sqrt{\langle\delta h^2\rangle}$, with membrane–substrate separation, h, as derived by Lipowsky *et al.*[6,54] They found different scaling behaviour for a low and a high tension regime, with both regimes being separated by a crossover length scale[6,54] $l_\sigma = \sqrt{k_B T/(2\pi\sigma)}$. We assumed a high tension regime with $l_\sigma > \sqrt{\langle\delta h^2\rangle}$ for vesicles exposed to osmotic differences of 20 mOsm l^{-1}, as here events of unspecific adhesion were observed. The lack of fluctuations yielded $\sqrt{\langle\delta h^2\rangle}$¡ 6 nm (as defined by the noise threshold). Inserting 6 nm in the above inequality and solving for σ resulted in a minimal possible tension in this regime of $\sigma_{min} = 18$ μJ m^{-2}. For vesicles exposed to the high osmotic gradients of 120, 145 and 170 mOsm l^{-1}, low tension was assumed. In this case the measured fluctuations follow $l_\sigma < \sqrt{\langle\delta h^2\rangle}$, permitting, with $\sqrt{\langle\delta h^2\rangle} = 17$nm, a maximal tension of $\sigma_{max} = 2$ μJ m^{-2}.
52 R. Bruinsma and E. Sackmann, *Comptes Rendus de l'Academie des Sciences*, 2001, **2**, 803–815.
53 R. R. Netz, *Phys. Rev. E: Stat. Phys., Plasmas, Fluids, Relat. Interdiscip. Top.*, 1995, **51**, 2286–2294.
54 R. R. Netz and R. Lipowsky, *Europhys. Lett.*, 1995, **29**, 345–350.

